Shale Attenuation

Prof. Christopher Liner
Associate director AGL

THE ATTENUATION CONSTANT OF EARTH MATERIALS*

W. T. BORN†

ABSTRACT

This paper discusses briefly the nature of viscous losses and solid friction losses, both of which may cause sound waves to be attenuated as they travel through a physical medium. A simple experimental technique for determining the nature and magnitude of the loss factor in small rock samples is described, and data are given which indicate that solid friction losses are primarily responsible for the observed attenuation of the seismic waves employed in the seismic reflection method.

A method of estimating the attenuation factor of earth materials from seismic reflection records is outlined and it is shown that the values so obtained are not inconsistent with the laboratory data.

Frequency characteristic curves of seismic wave paths are derived on the basis of the experimental data.

1941

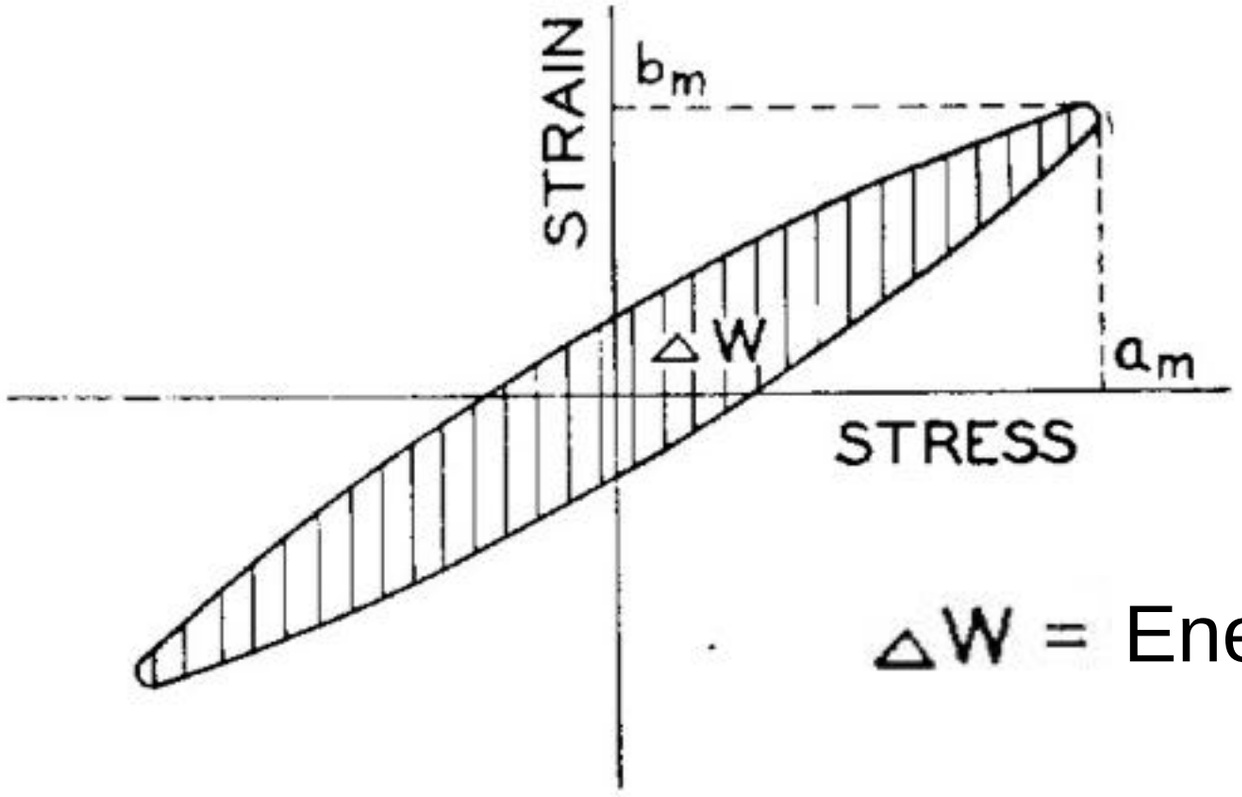

$\triangle W$ = Energy loss per cycle

SOLID FRICTION

$$\triangle W = K a_m^2 = K b_m^2 E^2$$

WHERE

K = SOLID FRICTION FACTOR

E = ELASTIC CONSTANT

a_m = MAXIMUM STRESS

b_m = MAXIMUM DISPLACEMENT

VISCOUS DAMPING

$$\triangle W = K' a_m^2 f = K' b_m^2 E^2 f$$

WHERE

K' = VISCOUS LOSS FACTOR

f = FREQUENCY

FIG. 1. Stress-strain diagram.

A NOTE ON THE DETERMINATION OF THE VISCOSITY OF SHALE FROM THE MEASUREMENT OF WAVELET BREADTH*

NORMAN RICKER†

ABSTRACT

From the breadth of a wavelet for a given travel time, it is possible to calculate the viscosity of the formation through which the seismic disturbance has passed. This calculation has been carried out for the Cretaceous Shale of Eastern Colorado, and the value thus found ranges from 2.7×10^7 to 4.9×10^7, with a mean value of 3.8×10^7 grams per cm. per second.

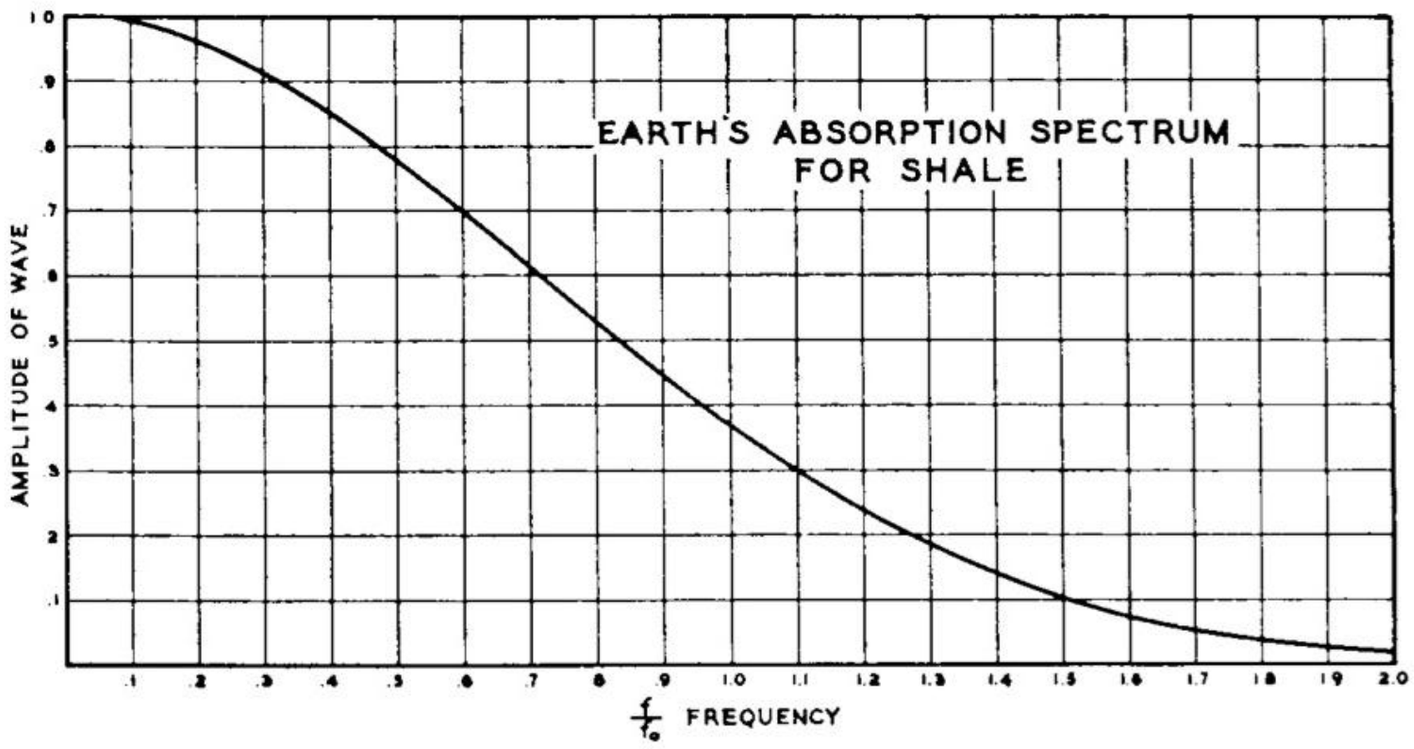

1941

VOLUME XXIII JULY, 1958 NUMBER 3

GEOPHYSICS

ATTENUATION OF SHEAR AND COMPRESSIONAL WAVES IN PIERRE SHALE*

F. J. McDONAL,† F. A. ANGONA,† R. L. MILLS,‡ R. L. SENGBUSH,†
R. G. VAN NOSTRAND,§ AND J. E. WHITE¶

ABSTRACT

Attenuation measurements were made near Limon, Colorado, where the Pierre shale is unusually uniform from depths of less than 100 ft to approximately 4,000 ft. Particle velocity wave forms were measured at distances up to 750 ft from explosive and mechanical sources. Explosives gave a well-defined compressional pulse which was observed along vertical and horizontal travel paths. A weight dropped on the bottom of a borehole gave a horizontally-traveling shear wave with vertical particle motion. In each case, signals from three-component clusters of geophones rigidly clamped in boreholes were amplified by a calibrated, wide-band system and recorded oscillographically. The frequency content of each wave form was obtained by Fourier analysis, and attenuation as a function of frequency was computed from these spectra.

For vertically-traveling compressional waves, an average of 6 determinations over the frequency range of 50–450 cps gives $\alpha = 0.12$ f. For horizontally-traveling shear waves with vertical motion in the frequency range 20–125 cps, the results are expressed by $\alpha = 1.0$ f. In each case attenuation is expressed in decibels per 1,000 ft of travel and f is frequency in cps. These measurements indicate, therefore, that the Pierre shale does not behave as a visco-elastic material.

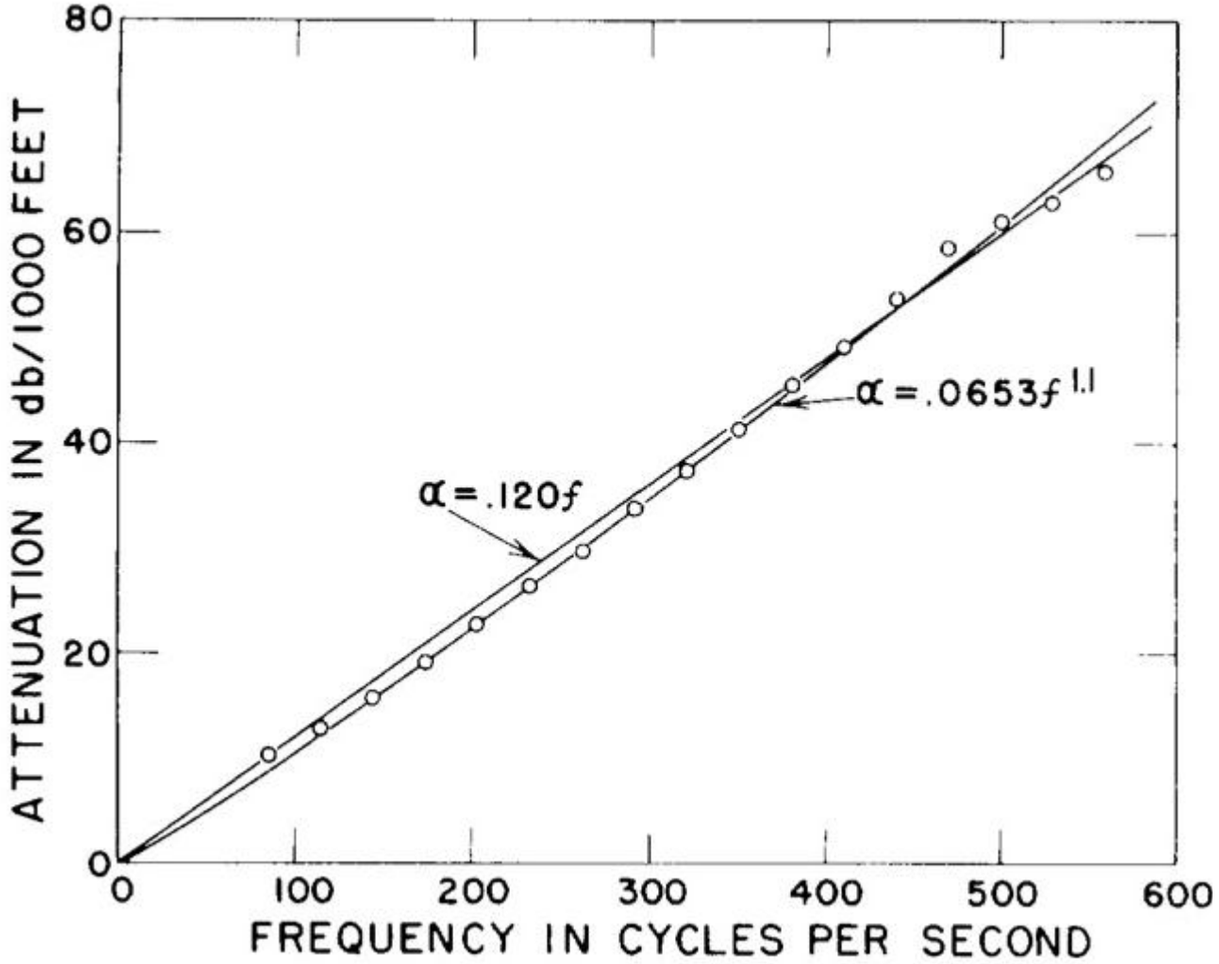
ATTENUATION IN db/1000 FEET
80
60
40
20
0
0
100
200
300
400
500
600
FREQUENCY IN CYCLES PER SECOND
α = .120f
α = .0653f 1.1

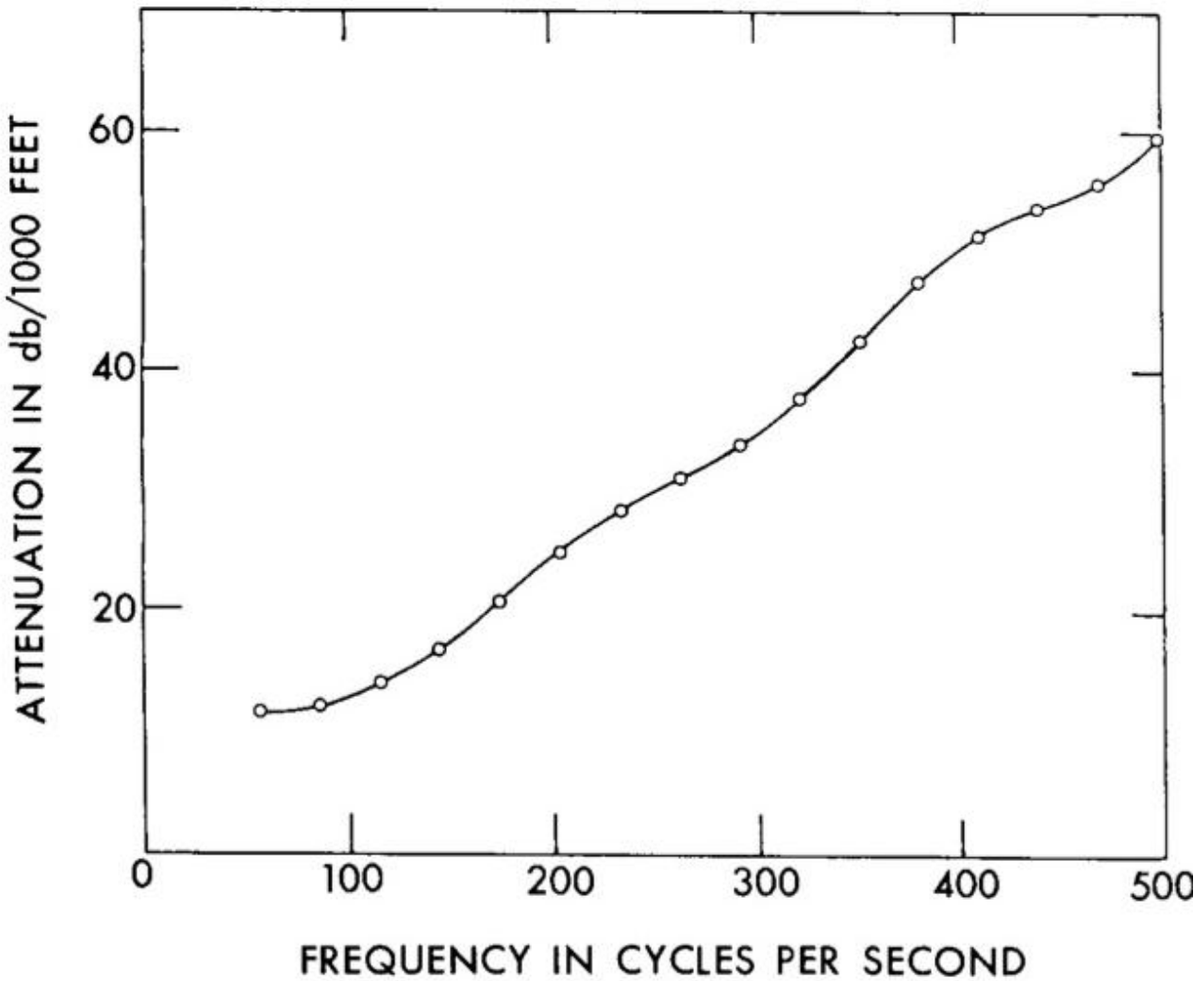
ATTENUATION IN db/1000 FEET
60
40
20
0
100
200
300
400
500
FREQUENCY IN CYCLES PER SECOND

GEOPHYSICS, VOL. XXIV, NO. 4 (OCTOBER, 1959), PP. 667–680, 8 FIGS.

A LOSS MECHANISM FOR THE PIERRE SHALE*

C. W. HORTON†

ABSTRACT

A theoretical study is made of a fairly simple model of an elastic solid in which losses are attributed to both the shear modulus and the bulk modulus. Each of these elastic parameters is represented by a circuit containing two springs and one dashpot. This is a modification of the usual Kelvin solid that has finite stiffness at infinite frequency. The four relaxation times introduced in the model are determined to fit the experimental data presented by McDonal *et al.* (1958). It is shown that one can obtain a very good representation of their experimental data with the model described above. The wave equation for an elastic solid is given in a canonical form so that one can compare easily the behavior of different models of the elastic parameters.

TABLE II. PARAMETERS OF THE CANONICAL WAVE EQUATION FOR VARIOUS ELASTIC MODELS

a. $F(x) = x^2/(1 + x^2)$

b. $G(x) = x/(1 + x^2)$

c. $V_p^{(0)} = \left[k^{(0)} + \frac{4}{3}\mu^{(0)}\right] \Big/ \rho$

d. $V_s^{(0)^2} = \mu^{(0)}/\rho$

e. For Maxwell liquid

$V_p^{(0)^2} = k^{(0)}/\rho$

$V_s^{(0)} = 0$

f. $P = \left[1 - \frac{4}{3}\left(\frac{V_s^{(0)}}{V_p^{(0)}}\right)^2\right]\frac{\tau_1 - \tau_2}{\tau_2}$

MODEL	IDEAL		KELVIN SOLID		MAXWELL LIQUID		MODIFIED KELVIN		PRESENT MODEL	
MODULUS	$\mathfrak{K}$	μ	$\mathfrak{K}$	μ	$\mathfrak{K}$	μ	$\mathfrak{K}$	μ	$\mathfrak{K}$	μ
MECHANICAL DIAGRAM Springs & dashpots				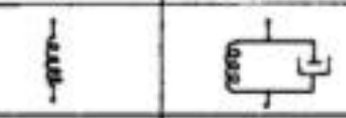				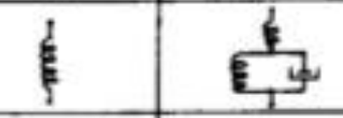	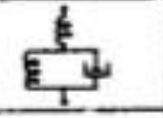	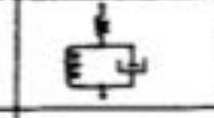
ELECTRIC DIAGRAM		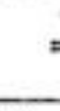		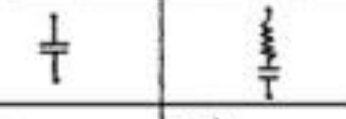		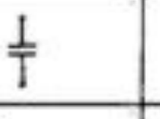		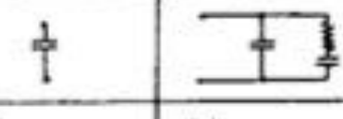	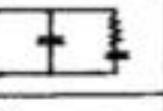	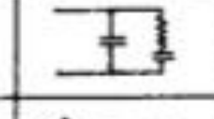
RESPONSE TO HEAVISIDE STRESS			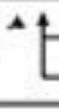	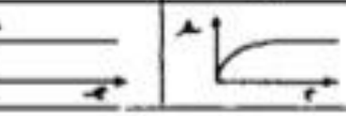	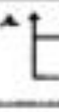	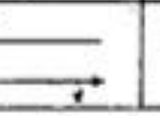		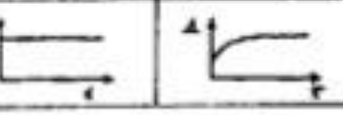	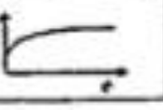	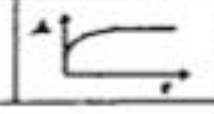
DEVIATORIC EQ.	$P_{ij} = 2\mu E_{ij}$		$P_{ij} = 2\mu\left[E_{ij} + \tau_3 \frac{dE_{ij}}{dt}\right]$		$2\mu_M \frac{dE_{ij}}{dt} = \frac{dP_{ij}}{dt} + \frac{1}{\tau_3} P_{ij}$		$P_{ij} + \tau_4 \frac{dP_{ij}}{dt} = 2\mu\left[E_{ij} + \tau_3 \frac{dE_{ij}}{dt}\right]$		$P_{ij} + \tau_4 \frac{dP_{ij}}{dt} = 2\mu\left[E_{ij} + \tau_3 \frac{dE_{ij}}{dt}\right]$	
$\mathfrak{K}(\omega)$ and $\mu(\omega)$ for $\exp(-i\omega t)$	$\mathfrak{K}^{(\omega)}$	$\mu^{(\omega)}$	$\mathfrak{K}^{(\omega)}$	$\mu^{(\omega)}(1 - i\omega\tau_3)$	$\mathfrak{K}^{(\omega)}$	$\mu_M\left\{\frac{-i\omega\tau_3}{1 - i\omega\tau_3}\right\}$	$\mathfrak{K}^{(\omega)}$	$\mu^{(\omega)}\left\{\frac{1 - i\omega\tau_3}{1 - i\omega\tau_4}\right\}$	$\mathfrak{K}^{(\omega)}\left\{\frac{1 - i\omega\tau_1}{1 - i\omega\tau_2}\right\}$	$\mu^{(\omega)}\left\{\frac{1 - i\omega\tau_3}{1 - i\omega\tau_4}\right\}$
$\mathfrak{K}^{(R)}$ and $\mu^{(R)}$ i.e., lim as $\omega \to \infty$	$\mathfrak{K}^{(\omega)}$	$\mu^{(\omega)}$	$\mathfrak{K}^{(\omega)}$	$-i\infty$	$\mathfrak{K}^{(\omega)}$	μ_M	$\mathfrak{K}^{(\omega)}$	$(\tau_3/\tau_4)\mu^{(\omega)}$	$(\tau_1/\tau_2)\mathfrak{K}^{(\omega)}$	$(\tau_3/\tau_4)\mu^{(\omega)}$
$A(\omega)$ see note a	1		1		$1 + P' F(\omega\tau_3)$		$1 + P' F(\omega\tau_4)$		$1 + P F(\omega\tau_2) + P' F(\omega\tau_4)$ see note f	
$B(\omega)$ see note b	0		$P'\omega\tau_3$		$P' G(\omega\tau_3)$		$P' G(\omega\tau_4)$		$P G(\omega\tau_2) + P' G(\omega\tau_4)$ see note f	
P'	—		$\frac{4}{3}\left[\frac{V_s^{(\omega)}}{V_p^{(\omega)}}\right]^2$		$\frac{4}{3}\frac{\mu_M}{\mathfrak{K}^{(\omega)}}$ see note e		$\frac{4}{3}\left[\frac{V_s^{(\omega)}}{V_p^{(\omega)}}\right]^2 \frac{\tau_3 - \tau_4}{\tau_4}$		$\frac{4}{3}\left[\frac{V_s^{(\omega)}}{V_p^{(\omega)}}\right]^2 \frac{\tau_3 - \tau_4}{\tau_4}$	
$V_p^{(R)}$ see note c	$V_p^{(\omega)}$		∞		$V_p^{(\omega)}\sqrt{1 + P'}$ see note e		$V_p^{(\omega)}\sqrt{1 + P'}$		$V_p^{(\omega)}\sqrt{1 + P + P'}$	
$A(\omega)^*$	1		1		$F(\omega\tau_3)$		$1 + Q F(\omega\tau_4)$		$1 + Q F(\omega\tau_4)$	
$B(\omega)^*$	0		$\omega\tau_3$		$G(\omega\tau_3)$		$Q G(\omega\tau_4)$		$Q G(\omega\tau_4)$	
Q	—		—		—		$(\tau_3 - \tau_4)/\tau_4$		$(\tau_3 - \tau_4)/\tau_4$	
$V_s^{(R)}$ see note d	$V_s^{(\omega)}$		∞		$[\mu_M/\rho]^{1/2}$ see note e		$V_s^{(\omega)}\sqrt{1 + Q}$		$V_s^{(\omega)}\sqrt{1 + Q}$	

GEOPHYSICS, VOL. 50, NO. 4 (APRIL 1985); P. 615-626, 16 FIGS.

Q estimation from vertical seismic profile data and anomalous variations in the central North Sea

S. D. Stainsby* and M. H. Worthington‡

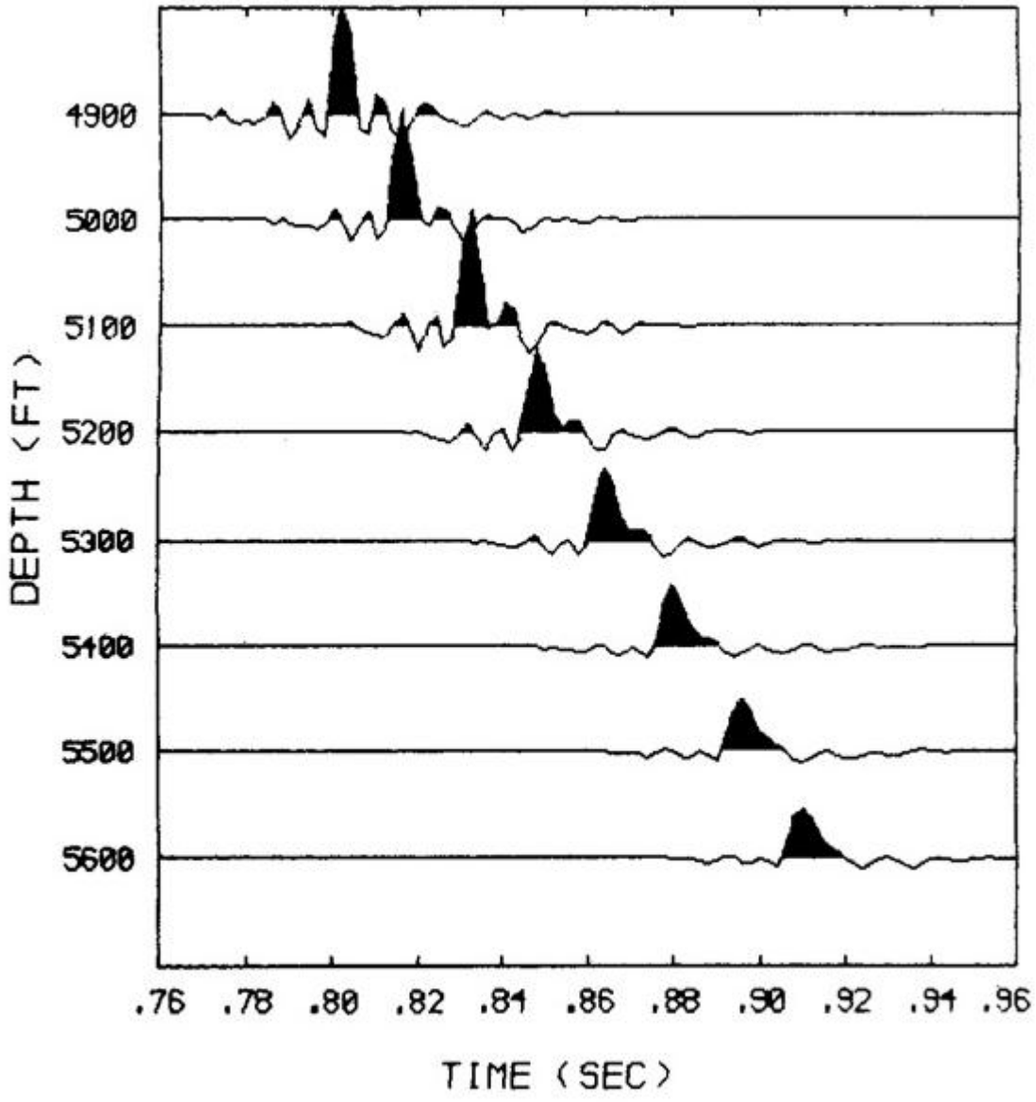

FIG. 8. Gain normalized traces from 4 900 to 5 600 ft showing decay in peak amplitude and asymmetry of attenuated impulse.

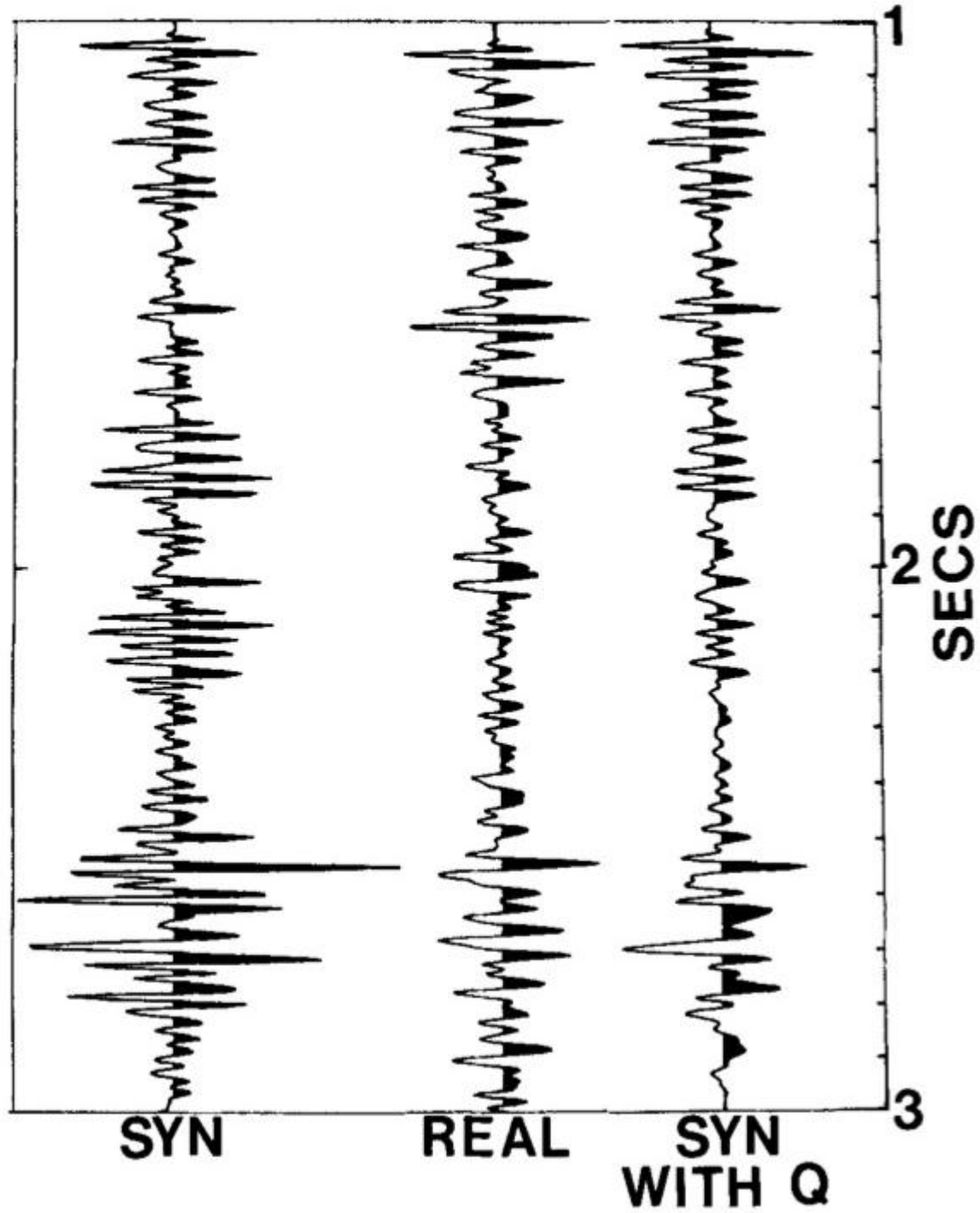

GEOPHYSICS, VOL. 63, NO. 2 (MARCH-APRIL 1998); P. 465–478, 17 FIGS., 1 TABLE.

Ultrasonic attenuation in Glenn Pool rocks, northeastern Oklahoma

Andrew P. Shatilo*, Carl Sondergeld‡, and Chandra S. Rai‡

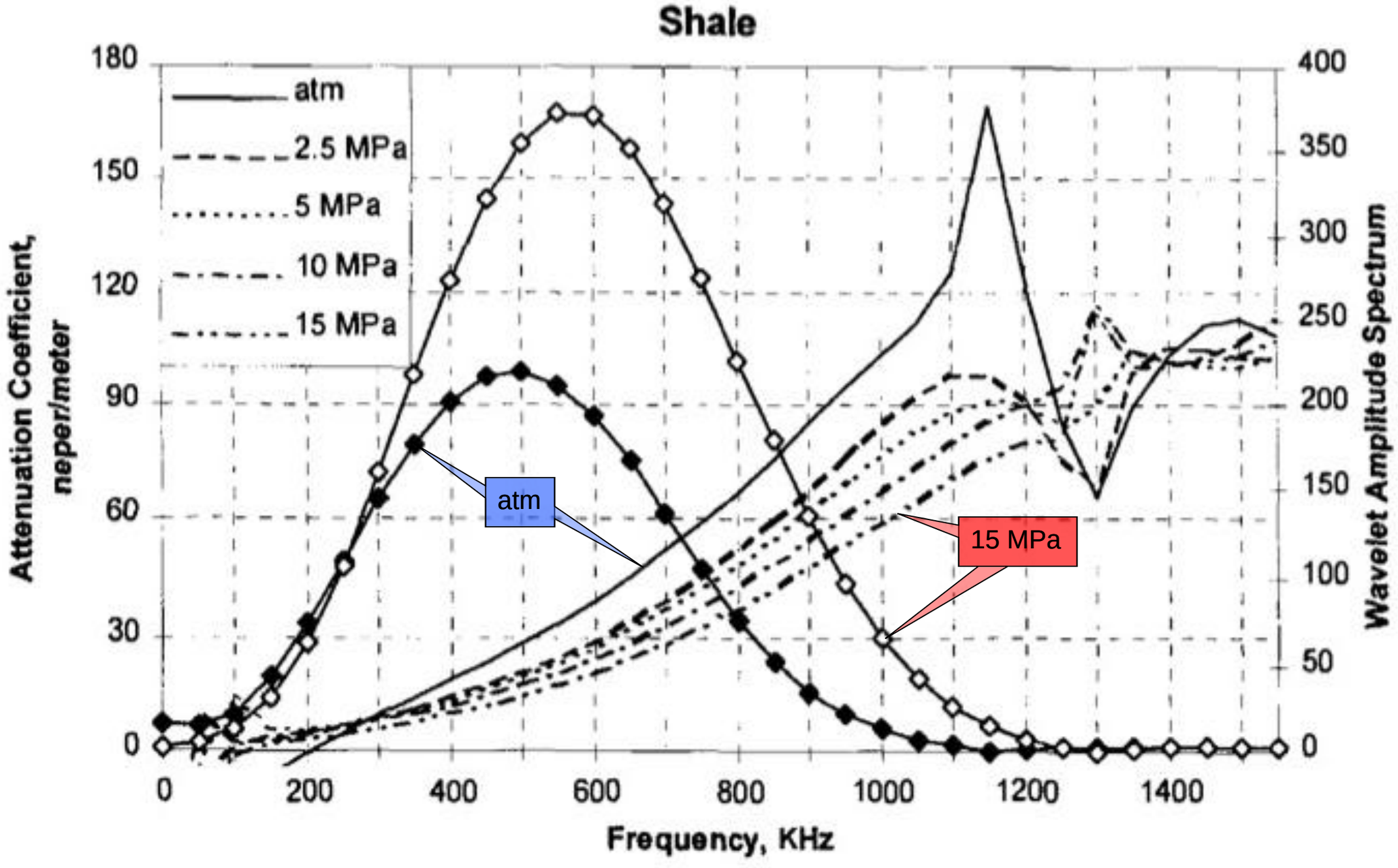

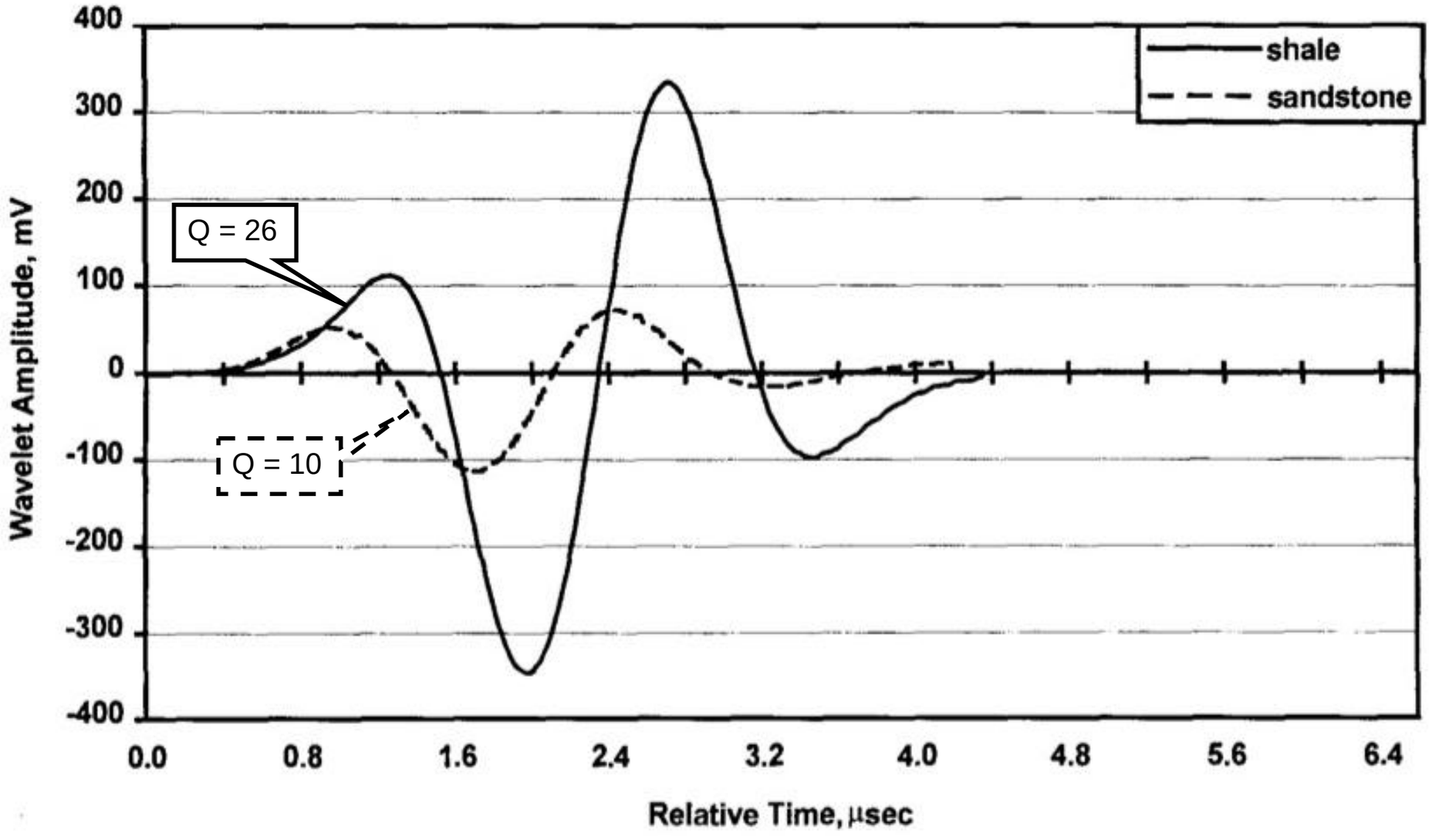

Experimental waveforms at an effective pressure of 5 MPa. Shale (sample no. 12): $Q = 26$, length = 36.3 mm. Sandston (sample no. 52): porosity = 13.4%, $Q = 10$, length = 38.5 mm.

AGL Data

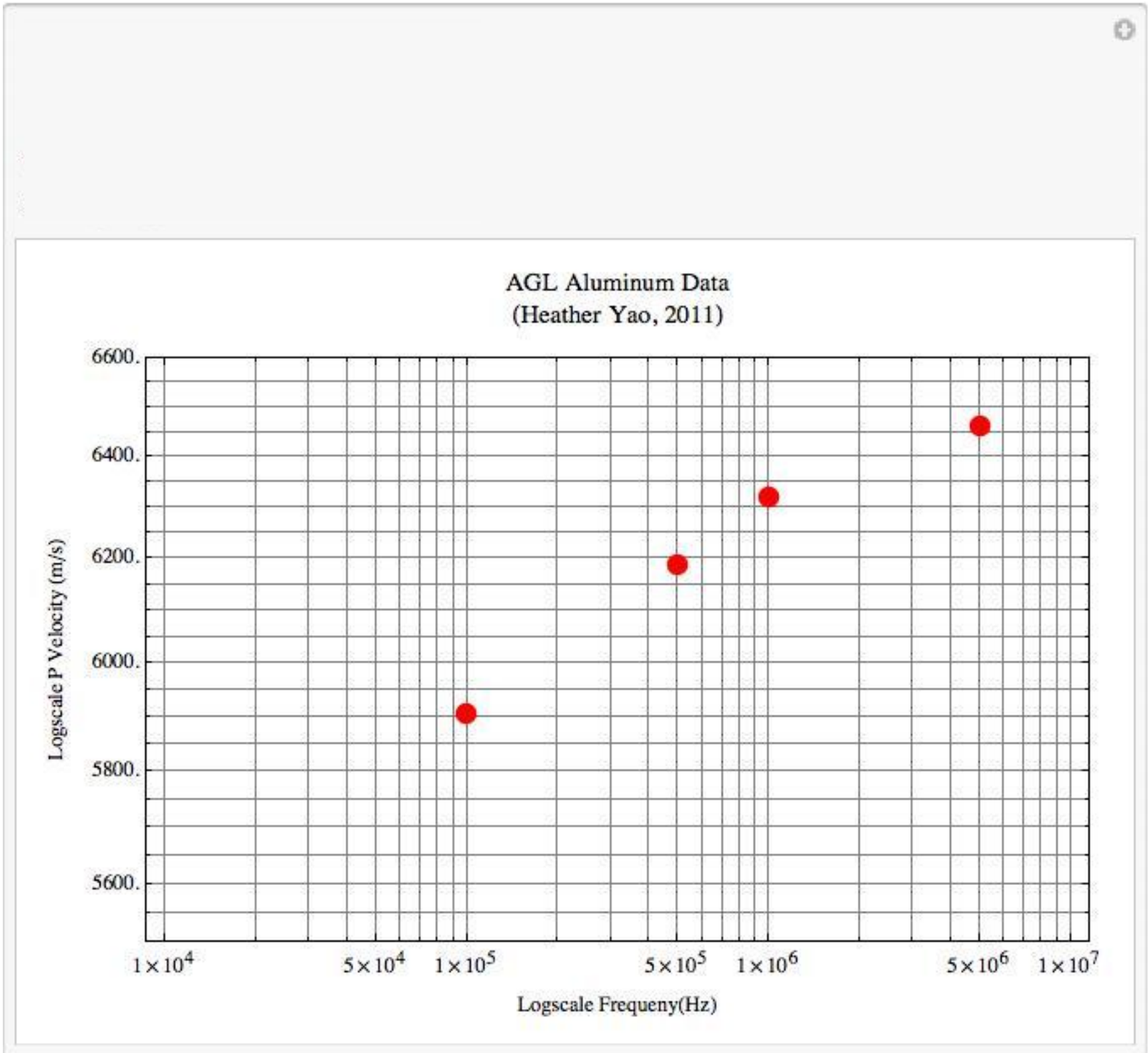
AGL Aluminum Data
(Heather Yao, 2011)
6600.
6400.
6200.
6000.
5800.
5600.
Logscale P Velocity (m/s)
1×10^4
5×10^4
1×10^5
5×10^5
1×10^6
5×10^6
1×10^7
Logscale Frequeny(Hz)

AGL Data

Q 15

f_0 in Hz 5000000

v_0 in m/s 6459

PlotRange 10000000

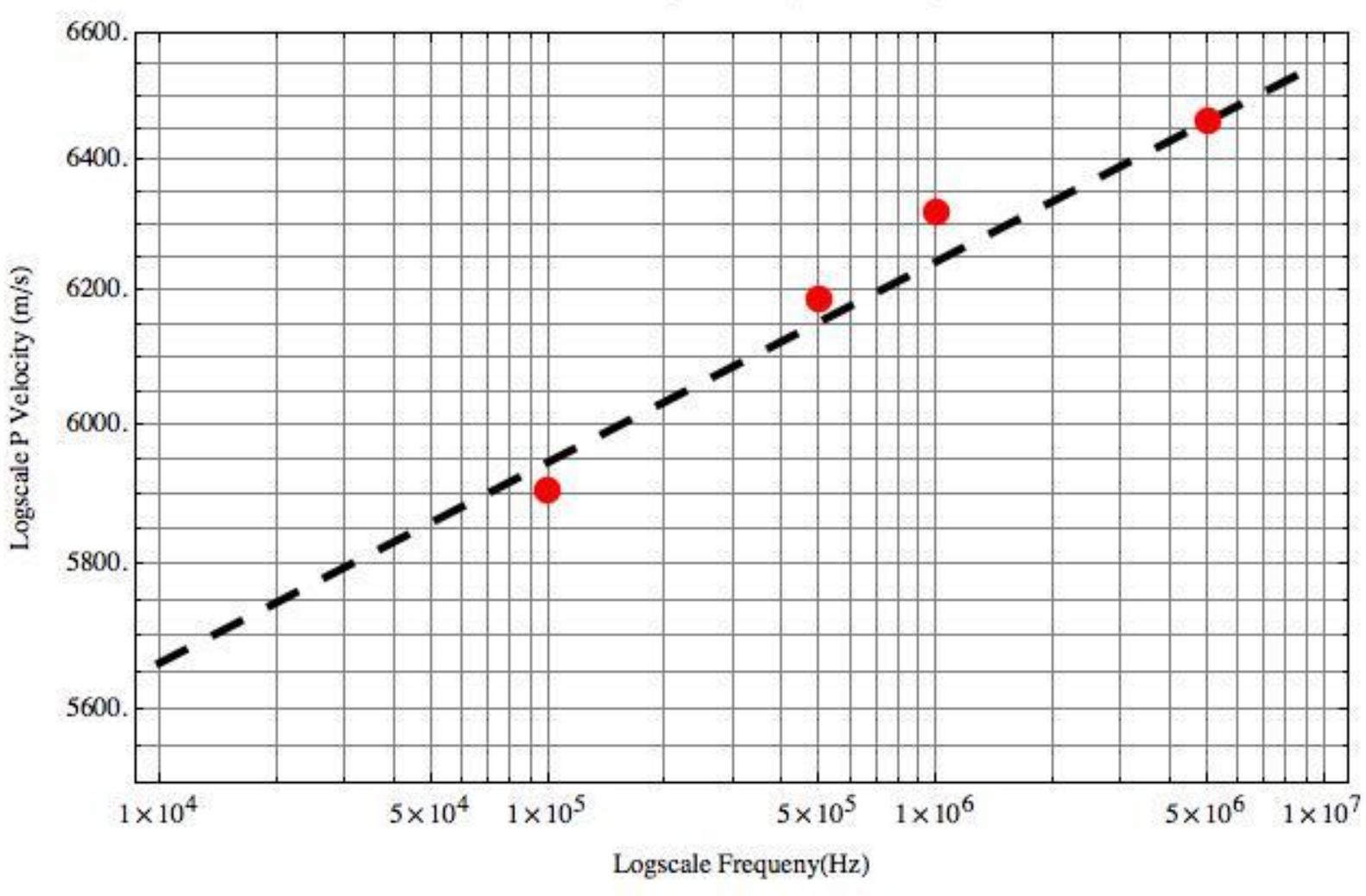

AGL Data

Static Velocity (m/s) 5905

Low Relaxation (Hz) 3000000

High Relaxation (Hz) 3600000

PlotRange 10000000

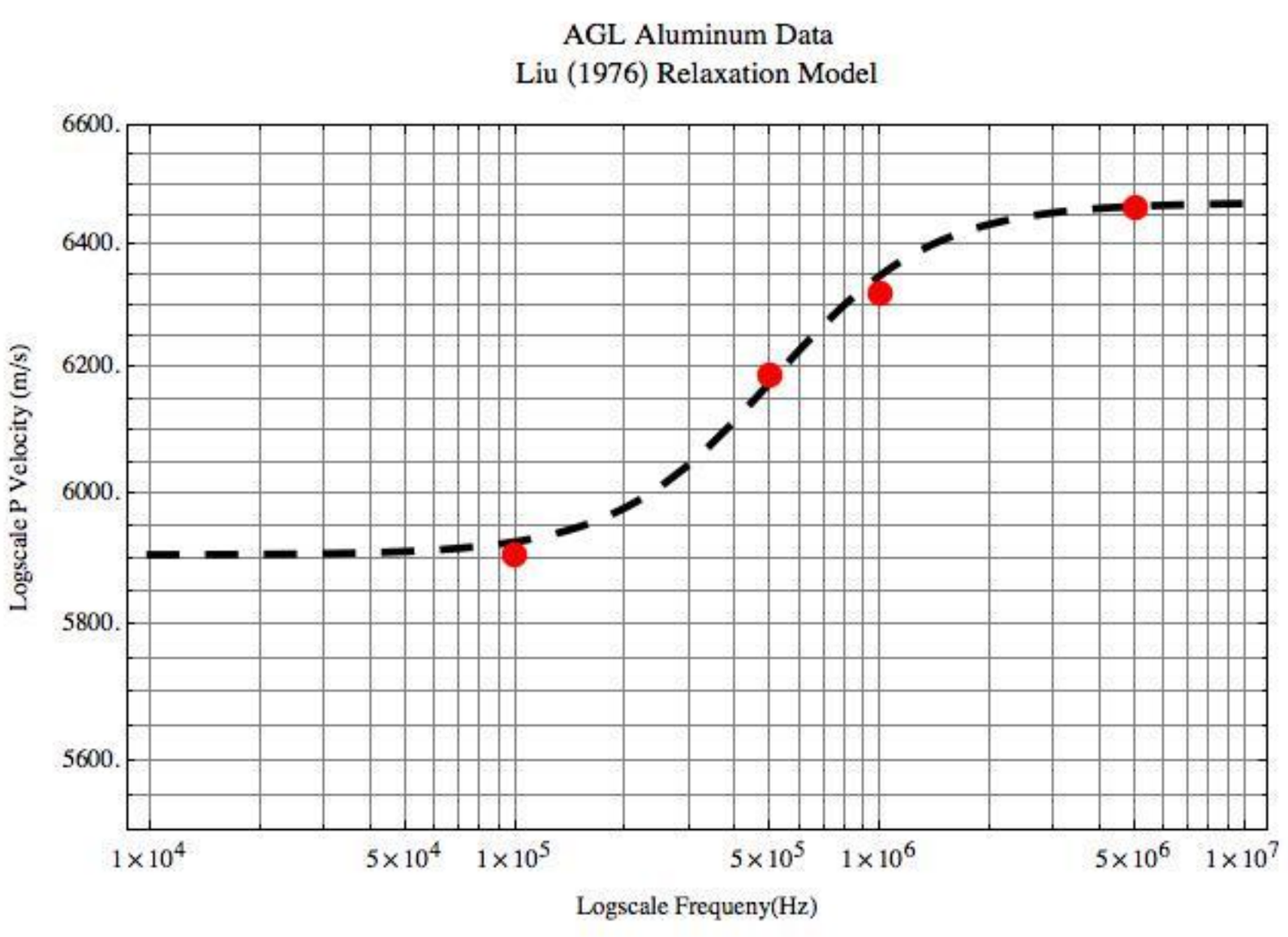

Thank You

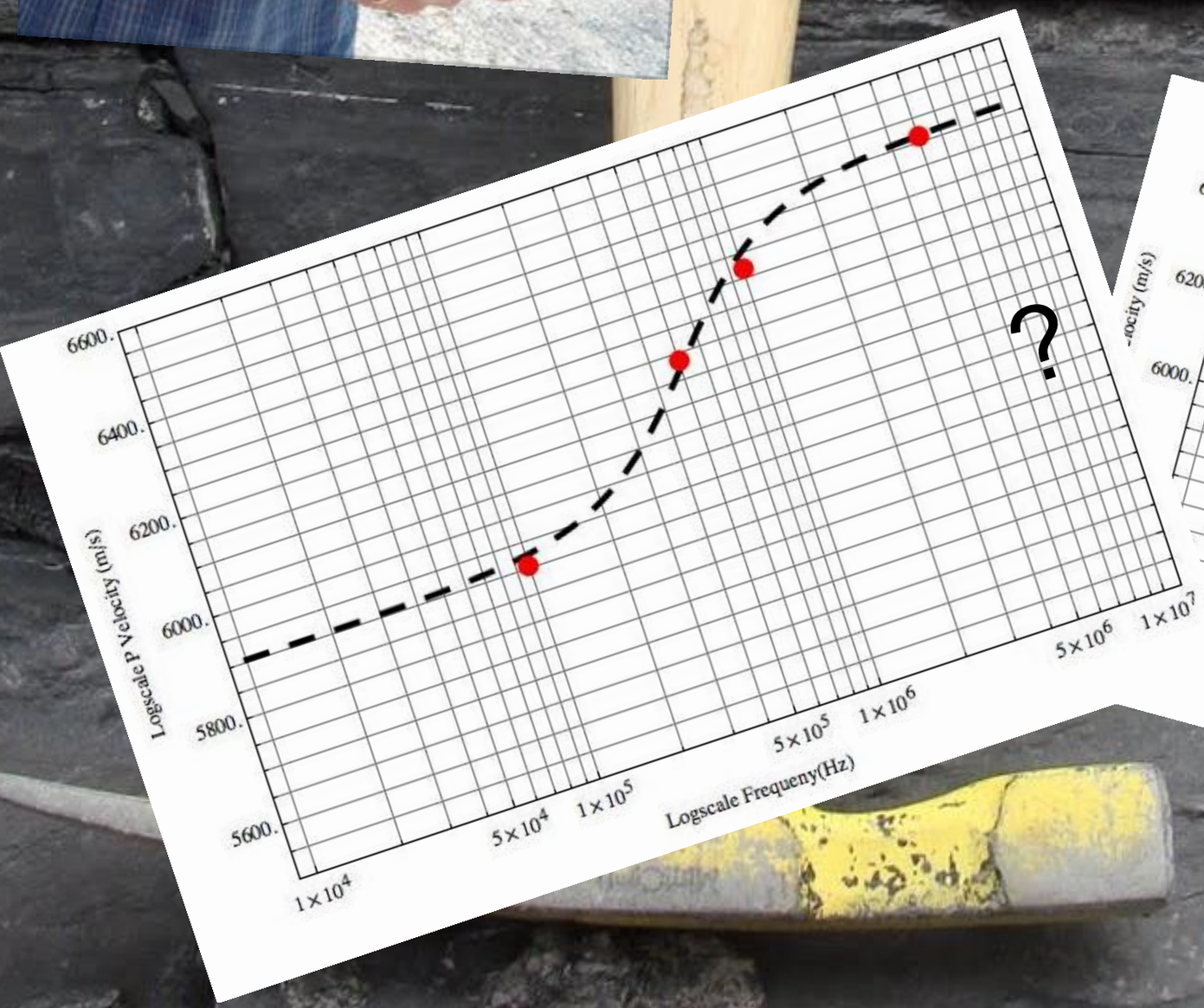
6600.
6400.
6200.
6000.
5800.
5600.
Logscale P Velocity (m/s)
1×10^4
5×10^4
1×10^5
5×10^5
1×10^6
5×10^6
1×10^7
Logscale Frequeny(Hz)
?

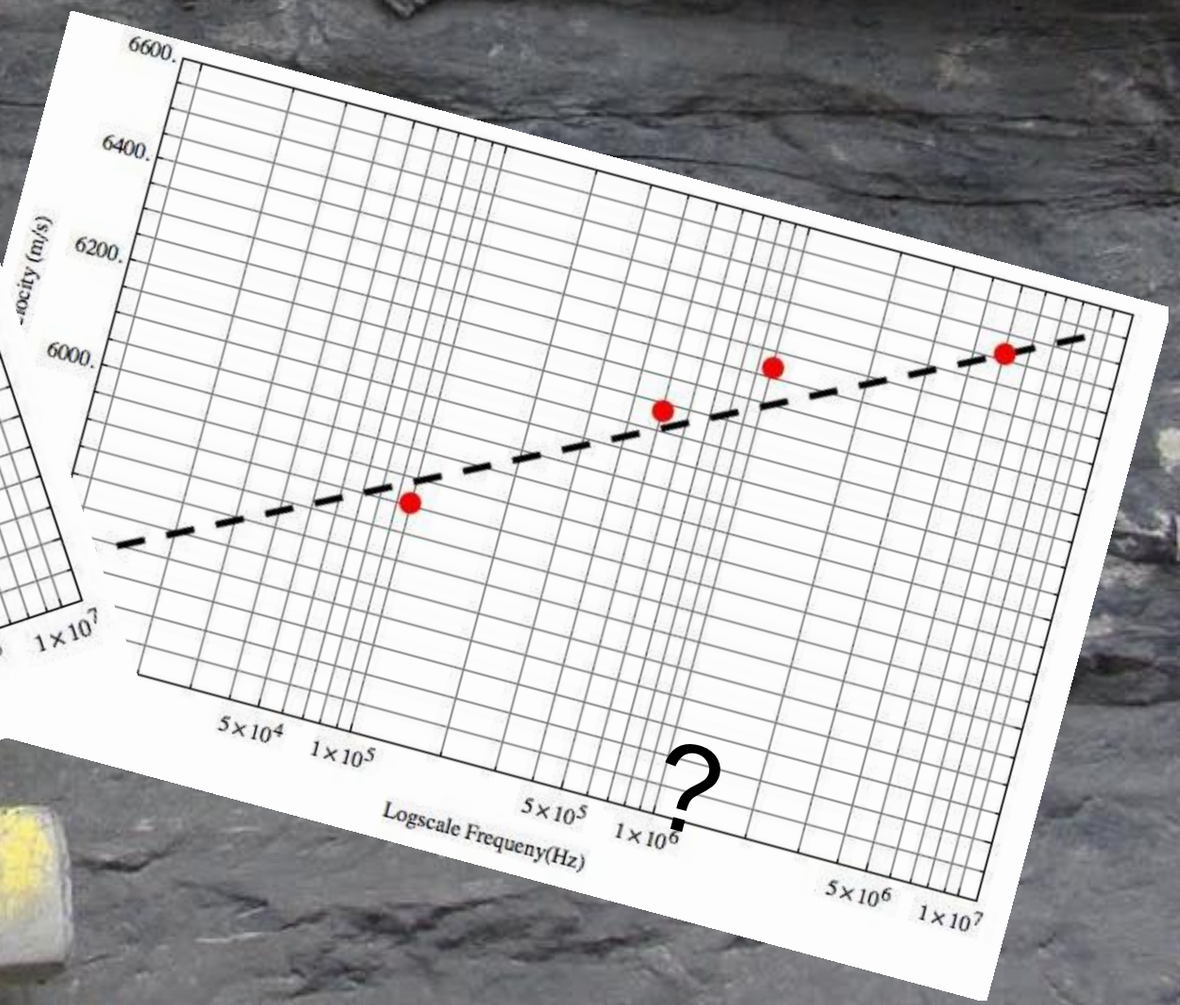
6600.
6400.
6200.
6000.
5×10^4
1×10^5
5×10^5
1×10^6
5×10^6
1×10^7
Logscale Frequeny(Hz)
?

Extra Slides

Sams et al. (1997) velocity data
Fit with Liu (1976) 2−parameter relaxation model

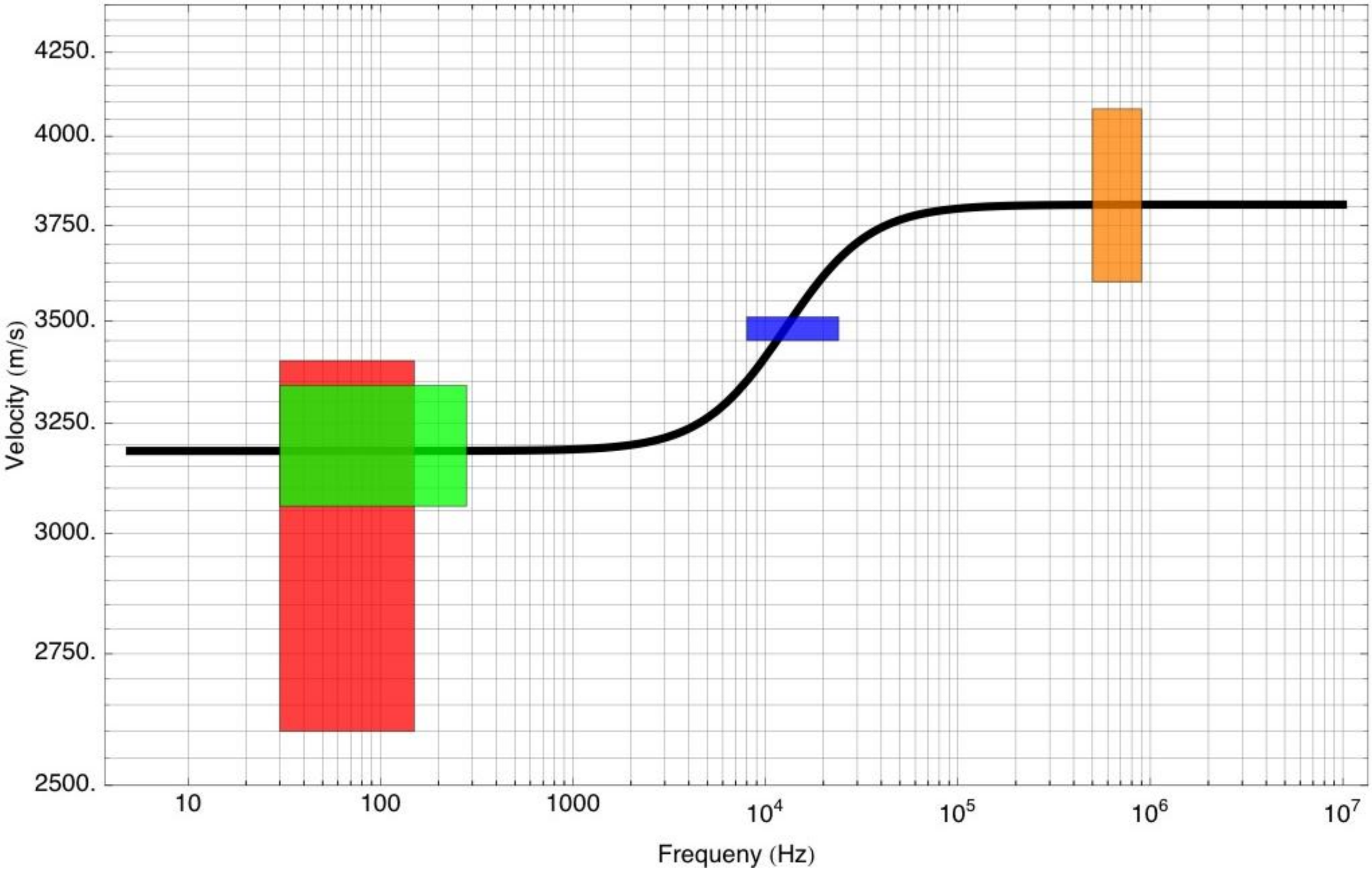

High porosity sandstone

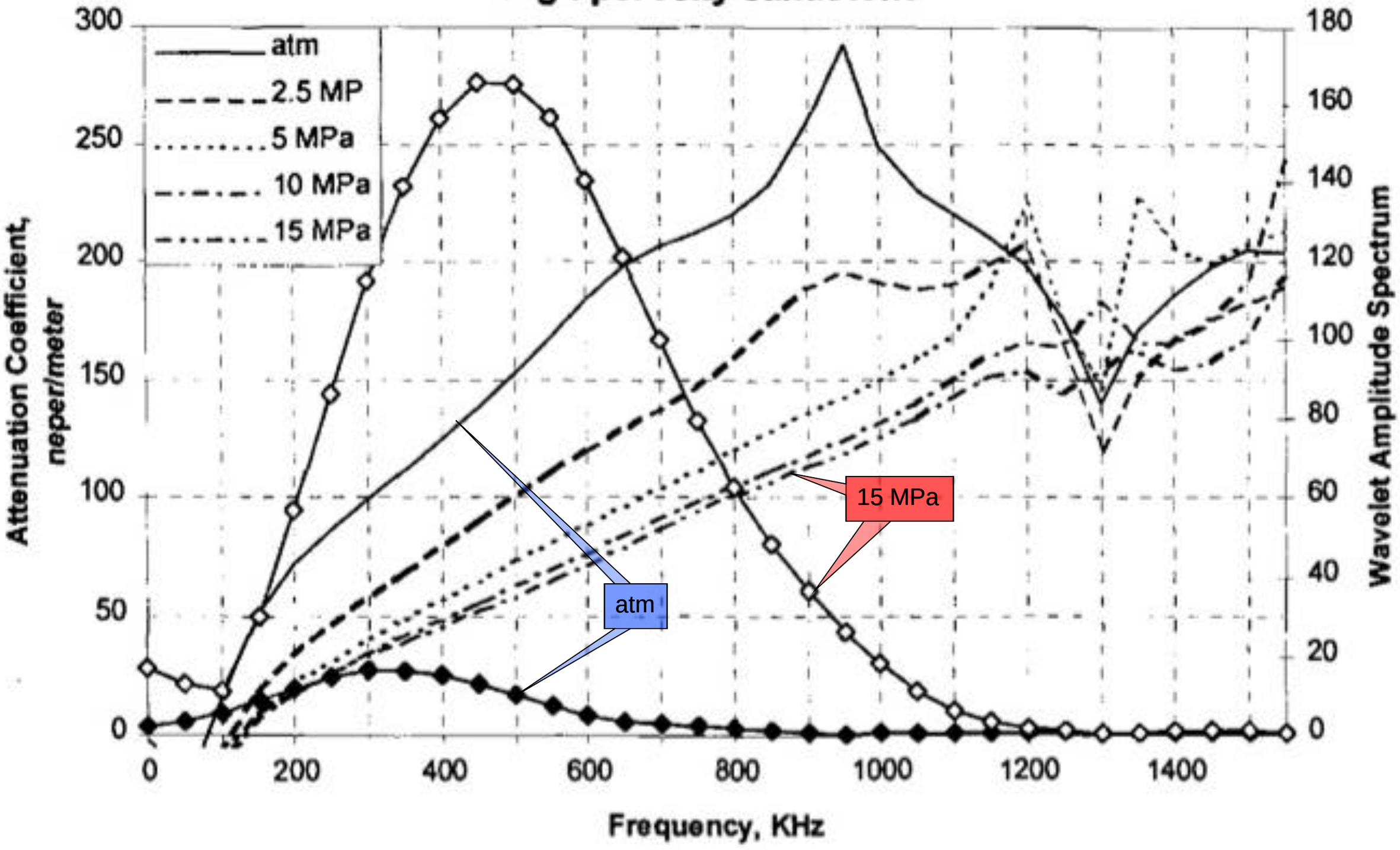

Low porosity sandstone

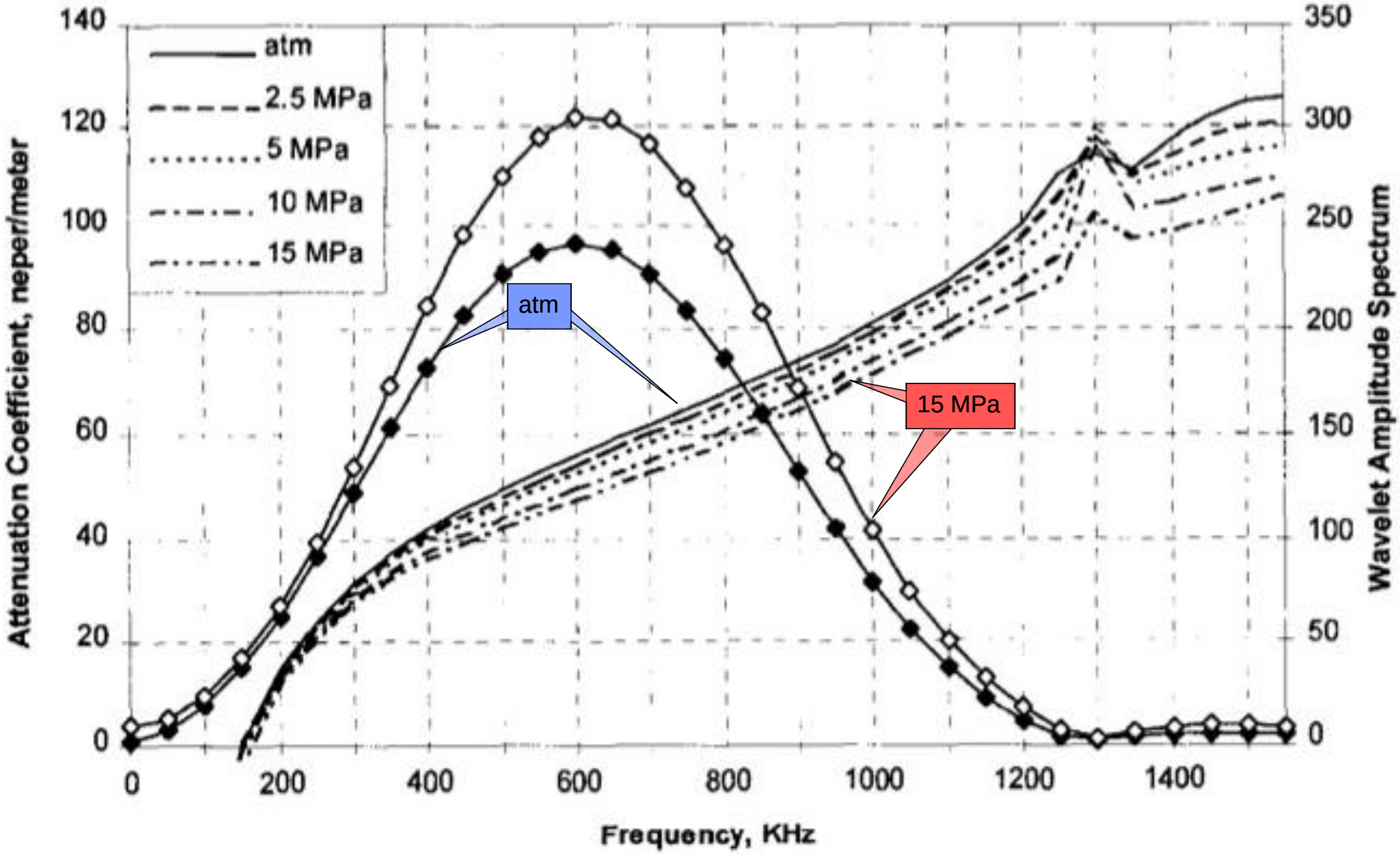

Shale

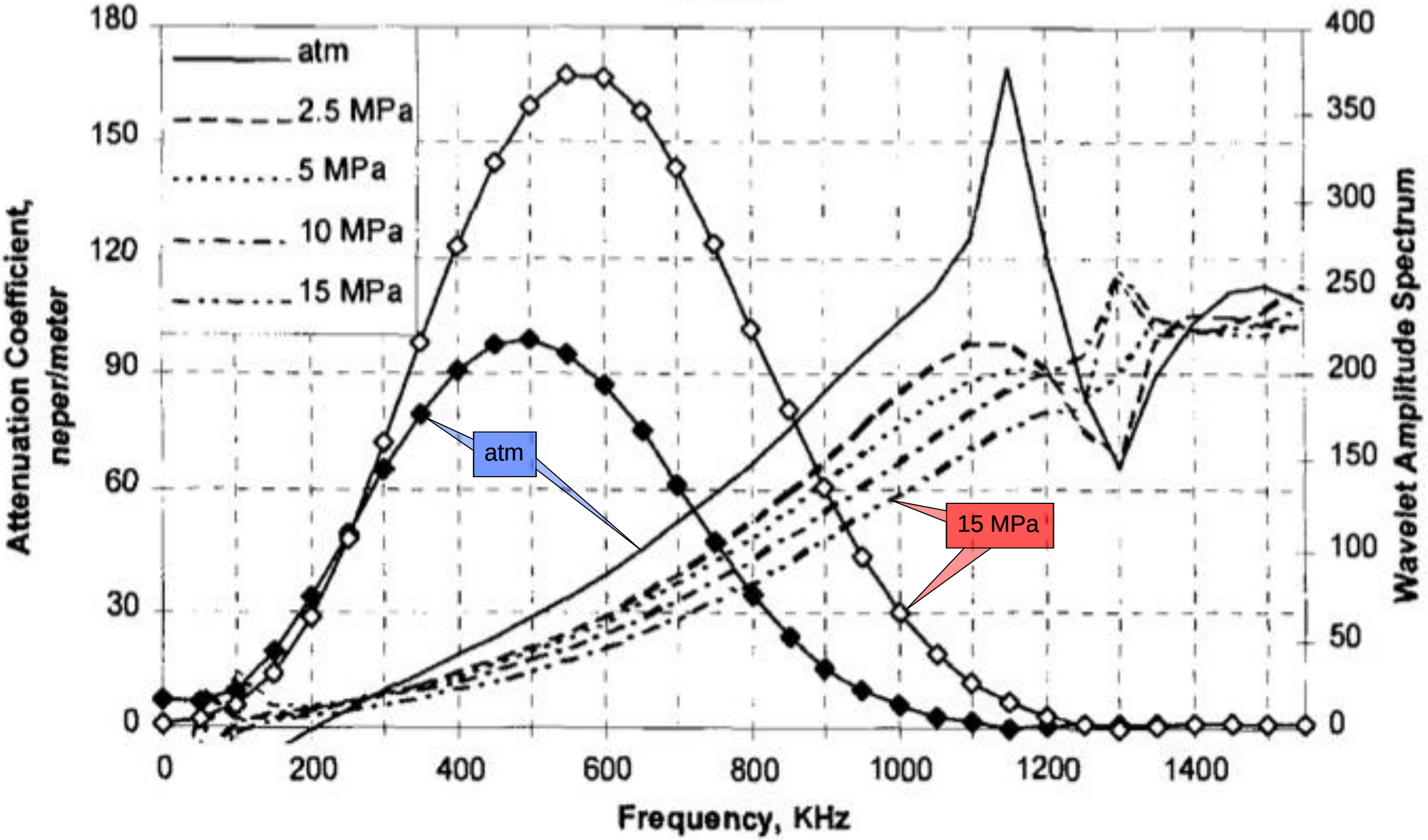
atm
2.5 MPa
5 MPa
10 MPa
15 MPa
Attenuation Coefficient, nepers/meter
Wavelet Amplitude Spectrum
Frequency, KHz
180
150
120
90
60
30
0
400
350
300
250
200
150
100
50
0
0
200
400
600
800
1000
1200
1400
atm
15 MPa